EUROPEAN ORGANIZATION FOR NUCLEAR RESEARCH

CERN–PH-EP/2004-068

03 September 2004

Production of Ξ_c^0 and Ξ_b in Z decays and lifetime measurement of Ξ_b

DELPHI Collaboration

Abstract

The charmed strange baryon Ξ_c^0 was searched for in the decay channel $\Xi_c^0 \to \Xi^-\pi^+$, and the beauty strange baryon Ξ_b in the inclusive channel $\Xi_b \to \Xi^-\ell^-\bar{\nu}X$, using the 3.5 million hadronic Z events collected by the DELPHI experiment in the years 1992–1995. The Ξ^- was reconstructed through the decay $\Xi^- \to \Lambda\pi^-$, using a constrained fit method for cascade decays. An iterative discriminant analysis was used for the Ξ_c^0 and Ξ_b selection. The production rates were measured to be $f_{\Xi_c^0}\times\mathrm{BR}(\Xi_c^0 \to \Xi^-\pi^+) = (4.7 \pm 1.4(stat.) \pm 1.1(syst.)) \times 10^{-4}$ per hadronic Z decay, and $\mathrm{BR}(b \to \Xi_b)\times\mathrm{BR}(\Xi_b \to \Xi^-\ell^-X) = (3.0 \pm 1.0(stat.) \pm 0.3(syst.)) \times 10^{-4}$ for each lepton species (electron or muon). The lifetime of the Ξ_b baryon was measured to be $\tau_{\Xi_b} = 1.45^{+0.55}_{-0.43}(stat.) \pm 0.13(syst.)$ ps. A combination with the previous DELPHI lifetime measurement gives $\tau_{\Xi_b} = 1.48^{+0.40}_{-0.31}(stat.) \pm 0.12(syst.)$ ps.

(Accepted by Euro. Phys. Journ. C)

J.Abdallah[25], P.Abreu[22], W.Adam[51], P.Adzic[11], T.Albrecht[17], T.Alderweireld[2], R.Alemany-Fernandez[8], T.Allmendinger[17], P.P.Allport[23], U.Amaldi[29], N.Amapane[45], S.Amato[48], E.Anashkin[36], A.Andreazza[28], S.Andringa[22], N.Anjos[22], P.Antilogus[25], W-D.Apel[17], Y.Arnoud[14], S.Ask[26], B.Asman[44], J.E.Augustin[25], A.Augustinus[8], P.Baillon[8], A.Ballestrero[46], P.Bambade[20], R.Barbier[27], D.Bardin[16], G.J.Barker[17], A.Baroncelli[39], M.Battaglia[8], M.Baubillier[25], K-H.Becks[53], M.Begalli[6], A.Behrmann[53], E.Ben-Haim[20], N.Benekos[32], A.Benvenuti[5], C.Berat[14], M.Berggren[25], L.Berntzon[44], D.Bertrand[2], M.Besancon[40], N.Besson[40], D.Bloch[9], M.Blom[31], M.Bluj[52], M.Bonesini[29], M.Boonekamp[40], P.S.L.Booth[23], G.Borisov[21], O.Botner[49], B.Bouquet[20], T.J.V.Bowcock[23], I.Boyko[16], M.Bracko[43], R.Brenner[49], E.Brodet[35], P.Bruckman[18], J.M.Brunet[7], P.Buschmann[53], M.Calvi[29], T.Camporesi[8], V.Canale[38], F.Carena[8], N.Castro[22], F.Cavallo[5], M.Chapkin[42], Ph.Charpentier[8], P.Checchia[36], R.Chierici[8], P.Chliapnikov[42], J.Chudoba[8], S.U.Chung[8], K.Cieslik[18], P.Collins[8], R.Contri[13], G.Cosme[20], F.Cossutti[47], M.J.Costa[50], D.Crennell[37], J.Cuevas[34], J.D'Hondt[2], J.Dalmau[44], T.da Silva[48], W.Da Silva[25], G.Della Ricca[47], A.De Angelis[47], W.De Boer[17], C.De Clercq[2], B.De Lotto[47], N.De Maria[45], A.De Min[36], L.de Paula[48], L.Di Ciaccio[38], A.Di Simone[39], K.Doroba[52], J.Drees[53,8], G.Eigen[4], T.Ekelof[49], M.Ellert[49], M.Elsing[8], M.C.Espirito Santo[22], G.Fanourakis[11], D.Fassouliotis[11,3], M.Feindt[17], J.Fernandez[41], A.Ferrer[50], F.Ferro[13], U.Flagmeyer[53], H.Foeth[8], E.Fokitis[32], F.Fulda-Quenzer[20], J.Fuster[50], M.Gandelman[48], C.Garcia[50], Ph.Gavillet[8], E.Gazis[32], R.Gokieli[8,52], B.Golob[43], G.Gomez-Ceballos[41], P.Goncalves[22], E.Graziani[39], G.Grosdidier[20], K.Grzelak[52], J.Guy[37], C.Haag[17], A.Hallgren[49], K.Hamacher[53], K.Hamilton[35], S.Haug[33], F.Hauler[17], V.Hedberg[26], M.Hennecke[17], H.Herr[†8], J.Hoffman[52], S-O.Holmgren[44], P.J.Holt[8], M.A.Houlden[23], K.Hultqvist[44], J.N.Jackson[23], G.Jarlskog[26], P.Jarry[40], D.Jeans[35], E.K.Johansson[44], P.D.Johansson[44], P.Jonsson[27], C.Joram[8], L.Jungermann[17], F.Kapusta[25], S.Katsanevas[27], E.Katsoufis[32], G.Kernel[43], B.P.Kersevan[8,43], U.Kerzel[17], B.T.King[23], N.J.Kjaer[8], P.Kluit[31], P.Kokkinias[11], C.Kourkoumelis[3], O.Kouznetsov[16], Z.Krumstein[16], M.Kucharczyk[18], J.Lamsa[1], G.Leder[51], F.Ledroit[14], L.Leinonen[44], R.Leitner[30], J.Lemonne[2], V.Lepeltier[20], T.Lesiak[18], W.Liebig[53], D.Liko[51], A.Lipniacka[44], J.H.Lopes[48], J.M.Lopez[34], D.Loukas[11], P.Lutz[40], L.Lyons[35], J.MacNaughton[51], A.Malek[53], S.Maltezos[32], F.Mandl[51], J.Marco[41], R.Marco[41], B.Marechal[48], M.Margoni[36], J-C.Marin[8], C.Mariotti[8], A.Markou[11], C.Martinez-Rivero[41], J.Masik[12], N.Mastroyiannopoulos[11], F.Matorras[41], C.Matteuzzi[29], F.Mazzucato[36], M.Mazzucato[36], R.Mc Nulty[23], C.Meroni[28], E.Migliore[45], W.Mitaroff[51], U.Mjoernmark[26], T.Moa[44], M.Moch[17], K.Moenig[8,10], R.Monge[13], J.Montenegro[31], D.Moraes[48], S.Moreno[22], P.Morettini[13], U.Mueller[53], K.Muenich[53], M.Mulders[31], L.Mundim[6], W.Murray[37], B.Muryn[19], G.Myatt[35], T.Myklebust[33], M.Nassiakou[11], F.Navarria[5], K.Nawrocki[52], R.Nicolaidou[40], M.Nikolenko[16,9], A.Oblakowska-Mucha[19], V.Obraztsov[42], A.Olshevski[16], A.Onofre[22], R.Orava[15], K.Osterberg[15], A.Ouraou[40], A.Oyanguren[50], M.Paganoni[29], S.Paiano[5], J.P.Palacios[23], H.Palka[18], Th.D.Papadopoulou[32], L.Pape[8], C.Parkes[24], F.Parodi[13], U.Parzefall[8], A.Passeri[39], O.Passon[53], L.Peralta[22], V.Perepelitsa[50], A.Perrotta[5], A.Petrolini[13], J.Piedra[41], L.Pieri[39], F.Pierre[40], M.Pimenta[22], E.Piotto[8], T.Podobnik[43], V.Poireau[8], M.E.Pol[6], G.Polok[18], V.Pozdniakov[16], N.Pukhaeva[2,16], A.Pullia[29], J.Rames[12], A.Read[33], P.Rebecchi[8], J.Rehn[17], D.Reid[31], R.Reinhardt[53], P.Renton[35], F.Richard[20], J.Ridky[12], M.Rivero[41], D.Rodriguez[41], A.Romero[45], P.Ronchese[36], P.Roudeau[20], T.Rovelli[5], V.Ruhlmann-Kleider[40], D.Ryabtchikov[42], A.Sadovsky[16], L.Salmi[15], J.Salt[50], C.Sander[17], A.Savoy-Navarro[25], U.Schwickerath[8], A.Segar[†35], R.Sekulin[37], M.Siebel[53], A.Sisakian[16], G.Smadja[27], O.Smirnova[26], A.Sokolov[42], A.Sopczak[21], R.Sosnowski[52], T.Spassov[8], M.Stanitzki[17], A.Stocchi[20], J.Strauss[51], B.Stugu[4], M.Szczekowski[52], M.Szeptycka[52], T.Szumlak[19], T.Tabarelli[29], A.C.Taffard[23], F.Tegenfeldt[49], J.Timmermans[31], L.Tkatchev[16], M.Tobin[23], S.Todorovova[12], B.Tome[22], A.Tonazzo[29], P.Tortosa[50], P.Travnicek[12], D.Treille[8], G.Tristram[7], M.Trochimczuk[52], C.Troncon[28], M-L.Turluer[40], I.A.Tyapkin[16], P.Tyapkin[16], S.Tzamarias[11], V.Uvarov[42], G.Valenti[5], P.Van Dam[31], J.Van Eldik[8], N.van Remortel[15], I.Van Vulpen[8], G.Vegni[28], F.Veloso[22], W.Venus[37], P.Verdier[27], V.Verzi[38], D.Vilanova[40], L.Vitale[47], V.Vrba[12], H.Wahlen[53], A.J.Washbrook[23], C.Weiser[17], D.Wicke[8], J.Wickens[2], G.Wilkinson[35], M.Winter[9], M.Witek[18], O.Yushchenko[42], A.Zalewska[18], P.Zalewski[52], D.Zavrtanik[43], V.Zhuravlov[16], N.I.Zimin[16], A.Zintchenko[16], M.Zupan[11]

[1]Department of Physics and Astronomy, Iowa State University, Ames IA 50011-3160, USA
[2]Physics Department, Universiteit Antwerpen, Universiteitsplein 1, B-2610 Antwerpen, Belgium
and IIHE, ULB-VUB, Pleinlaan 2, B-1050 Brussels, Belgium
and Faculté des Sciences, Univ. de l'Etat Mons, Av. Maistriau 19, B-7000 Mons, Belgium
[3]Physics Laboratory, University of Athens, Solonos Str. 104, GR-10680 Athens, Greece
[4]Department of Physics, University of Bergen, Allégaten 55, NO-5007 Bergen, Norway
[5]Dipartimento di Fisica, Università di Bologna and INFN, Via Irnerio 46, IT-40126 Bologna, Italy
[6]Centro Brasileiro de Pesquisas Físicas, rua Xavier Sigaud 150, BR-22290 Rio de Janeiro, Brazil
and Depto. de Física, Pont. Univ. Católica, C.P. 38071 BR-22453 Rio de Janeiro, Brazil
and Inst. de Física, Univ. Estadual do Rio de Janeiro, rua São Francisco Xavier 524, Rio de Janeiro, Brazil
[7]Collège de France, Lab. de Physique Corpusculaire, IN2P3-CNRS, FR-75231 Paris Cedex 05, France
[8]CERN, CH-1211 Geneva 23, Switzerland
[9]Institut de Recherches Subatomiques, IN2P3 - CNRS/ULP - BP20, FR-67037 Strasbourg Cedex, France
[10]Now at DESY-Zeuthen, Platanenallee 6, D-15735 Zeuthen, Germany
[11]Institute of Nuclear Physics, N.C.S.R. Demokritos, P.O. Box 60228, GR-15310 Athens, Greece
[12]FZU, Inst. of Phys. of the C.A.S. High Energy Physics Division, Na Slovance 2, CZ-180 40, Praha 8, Czech Republic
[13]Dipartimento di Fisica, Università di Genova and INFN, Via Dodecaneso 33, IT-16146 Genova, Italy
[14]Institut des Sciences Nucléaires, IN2P3-CNRS, Université de Grenoble 1, FR-38026 Grenoble Cedex, France
[15]Helsinki Institute of Physics and Department of Physical Sciences, P.O. Box 64, FIN-00014 University of Helsinki, Finland
[16]Joint Institute for Nuclear Research, Dubna, Head Post Office, P.O. Box 79, RU-101 000 Moscow, Russian Federation
[17]Institut für Experimentelle Kernphysik, Universität Karlsruhe, Postfach 6980, DE-76128 Karlsruhe, Germany
[18]Institute of Nuclear Physics PAN,Ul. Radzikowskiego 152, PL-31142 Krakow, Poland
[19]Faculty of Physics and Nuclear Techniques, University of Mining and Metallurgy, PL-30055 Krakow, Poland
[20]Université de Paris-Sud, Lab. de l'Accélérateur Linéaire, IN2P3-CNRS, Bât. 200, FR-91405 Orsay Cedex, France
[21]School of Physics and Chemistry, University of Lancaster, Lancaster LA1 4YB, UK
[22]LIP, IST, FCUL - Av. Elias Garcia, 14-1^o, PT-1000 Lisboa Codex, Portugal
[23]Department of Physics, University of Liverpool, P.O. Box 147, Liverpool L69 3BX, UK
[24]Dept. of Physics and Astronomy, Kelvin Building, University of Glasgow, Glasgow G12 8QQ
[25]LPNHE, IN2P3-CNRS, Univ. Paris VI et VII, Tour 33 (RdC), 4 place Jussieu, FR-75252 Paris Cedex 05, France
[26]Department of Physics, University of Lund, Sölvegatan 14, SE-223 63 Lund, Sweden
[27]Université Claude Bernard de Lyon, IPNL, IN2P3-CNRS, FR-69622 Villeurbanne Cedex, France
[28]Dipartimento di Fisica, Università di Milano and INFN-MILANO, Via Celoria 16, IT-20133 Milan, Italy
[29]Dipartimento di Fisica, Univ. di Milano-Bicocca and INFN-MILANO, Piazza della Scienza 2, IT-20126 Milan, Italy
[30]IPNP of MFF, Charles Univ., Areal MFF, V Holesovickach 2, CZ-180 00, Praha 8, Czech Republic
[31]NIKHEF, Postbus 41882, NL-1009 DB Amsterdam, The Netherlands
[32]National Technical University, Physics Department, Zografou Campus, GR-15773 Athens, Greece
[33]Physics Department, University of Oslo, Blindern, NO-0316 Oslo, Norway
[34]Dpto. Fisica, Univ. Oviedo, Avda. Calvo Sotelo s/n, ES-33007 Oviedo, Spain
[35]Department of Physics, University of Oxford, Keble Road, Oxford OX1 3RH, UK
[36]Dipartimento di Fisica, Università di Padova and INFN, Via Marzolo 8, IT-35131 Padua, Italy
[37]Rutherford Appleton Laboratory, Chilton, Didcot OX11 OQX, UK
[38]Dipartimento di Fisica, Università di Roma II and INFN, Tor Vergata, IT-00173 Rome, Italy
[39]Dipartimento di Fisica, Università di Roma III and INFN, Via della Vasca Navale 84, IT-00146 Rome, Italy
[40]DAPNIA/Service de Physique des Particules, CEA-Saclay, FR-91191 Gif-sur-Yvette Cedex, France
[41]Instituto de Fisica de Cantabria (CSIC-UC), Avda. los Castros s/n, ES-39006 Santander, Spain
[42]Inst. for High Energy Physics, Serpukov P.O. Box 35, Protvino, (Moscow Region), Russian Federation
[43]J. Stefan Institute, Jamova 39, SI-1000 Ljubljana, Slovenia and Laboratory for Astroparticle Physics,
Nova Gorica Polytechnic, Kostanjeviska 16a, SI-5000 Nova Gorica, Slovenia,
and Department of Physics, University of Ljubljana, SI-1000 Ljubljana, Slovenia
[44]Fysikum, Stockholm University, Box 6730, SE-113 85 Stockholm, Sweden
[45]Dipartimento di Fisica Sperimentale, Università di Torino and INFN, Via P. Giuria 1, IT-10125 Turin, Italy
[46]INFN,Sezione di Torino and Dipartimento di Fisica Teorica, Università di Torino, Via Giuria 1, IT-10125 Turin, Italy
[47]Dipartimento di Fisica, Università di Trieste and INFN, Via A. Valerio 2, IT-34127 Trieste, Italy
and Istituto di Fisica, Università di Udine, IT-33100 Udine, Italy
[48]Univ. Federal do Rio de Janeiro, C.P. 68528 Cidade Univ., Ilha do Fundão BR-21945-970 Rio de Janeiro, Brazil
[49]Department of Radiation Sciences, University of Uppsala, P.O. Box 535, SE-751 21 Uppsala, Sweden
[50]IFIC, Valencia-CSIC, and D.F.A.M.N., U. de Valencia, Avda. Dr. Moliner 50, ES-46100 Burjassot (Valencia), Spain
[51]Institut für Hochenergiephysik, Österr. Akad. d. Wissensch., Nikolsdorfergasse 18, AT-1050 Vienna, Austria
[52]Inst. Nuclear Studies and University of Warsaw, Ul. Hoza 69, PL-00681 Warsaw, Poland
[53]Fachbereich Physik, University of Wuppertal, Postfach 100 127, DE-42097 Wuppertal, Germany
[†] deceased

1 Introduction

Measuring the production rates of baryons, and heavy baryons in particular, is important in order to understand the underlying fragmentation process in $Z \to q\bar{q}$ events. The fragmentation process involves small momentum transfers and perturbation theory is not applicable, consequently no good theoretical description exists and phenomenological models have to be used. The production of a baryon-pair requires the creation of a di-quark pair in the fragmentation. The exact nature of the mechanism by which this occurs is still largely unknown. Thus the tuning of fragmentation models and the understanding of the processes involved in baryon production, require good measurements of the production of all the baryons in general, and baryons containing heavy quarks in particular.

In this paper, a first measurement of the production at the Z resonance of the charm strange baryon Ξ_c^0 is presented [1], using the exclusive decay channel $\Xi_c^0 \to \Xi^-\pi^+$. As a cross-check, the $\Xi(1530)^0$ resonance is reconstructed, through the decay channel $\Xi(1530)^0 \to \Xi^-\pi^+$.

A measurement of the production and lifetime of the strange b-baryon Ξ_b is also presented, using the semileptonic decay channel, $\Xi_b \to \Xi^-\ell^-\bar{\nu}X$. Here Ξ_b is used as a notation for the strange b-baryon states Ξ_b^- and Ξ_b^0. The Ξ_b baryon will decay to $X_c X \ell^-\bar{\nu}$ followed by $X_c \to \Xi^- X'$, where X_c is a charmed baryon which yields a Ξ^- hyperon. X_c is dominantly Ξ_c^0, thus the most common state in this decay channel is the Ξ_b^-.

A first observation of the Ξ_b baryon production and lifetime has been published by DELPHI, using a smaller data sample [1], and has been confirmed by ALEPH [2]. Here the full LEP1 data sample collected by the DELPHI experiment between the years 1992–1995 is used. In this paper, the background is determined from the data whereas simulation was used in the previous DELPHI analysis. The new lifetime measurement is statistically independent from the previous DELPHI measurement and relies on a different method.

A constrained multivertex fit has been performed to reconstruct the $\Xi^- \to \Lambda\pi^-$decay. For the Ξ_c^0, $\Xi(1530)^0$ and Ξ_b selections, an iterative discriminant analysis method has been applied.

2 The apparatus

The DELPHI detector is described in detail elsewhere [3,4]. The detectors most important for this analysis are the Vertex Detector (VD), the Inner Detector (ID), the Time Projection Chamber (TPC), and the Outer Detector (OD). For the lepton identification in the Ξ_b analysis the electromagnetic calorimeter (HPC) and the muon chambers were also used.

The VD consists of three concentric layers of silicon-strip detectors, located at radii of 6 cm, 9 cm and 11 cm from the beam axis. The polar angles [2] covered for particles crossing all three layers are $44° < \theta < 136°$. In 1994 and 1995, the first and third layers of the VD had double-sided readout and gave both $R\phi$ and z coordinates. The TPC is the main tracking device where charged-particle tracks are reconstructed in three dimensions for radii between 40 cm and 110 cm. The ID and OD are two drift chambers located at radii between 12 cm and 28 cm and between 198 cm and 206 cm, respectively, and provide additional points for the track reconstruction.

[1] Charge conjugated states are implied throughout this paper, unless otherwise stated.

[2] In the standard DELPHI coordinate system, the z axis is along the electron beam direction, the x axis points towards the center of LEP, and the y axis points upwards. The polar angle to the z axis is called θ and the azimuthal angle around the z axis is called ϕ; the radial coordinate is $R = \sqrt{x^2 + y^2}$.

The b-tagging package developed by the DELPHI collaboration [4,5] has been used to select $Z \to b\bar{b}$ events. The impact parameters of the charged-particle tracks, with respect to the primary vertex, have been used to build the probability that all tracks come from the primary vertex. Due to the long b-hadron lifetime, the probability distribution is peaked at zero for events containing b-quarks whereas it is flat for events containing light quarks only.

3 Event selection and simulation

Hadronic Z decays were selected by requiring at least four reconstructed charged particles and a total energy of these particles (assumed to be pions) larger than 12% of the centre-of-mass energy. The charged-particle tracks had to be longer than 30 cm in the TPC, with a momentum larger than 400 MeV/c and a polar angle between 20° and 160°. The polar angle of the thrust axis, θ_{thrust}, was computed for each event and events were rejected if $|\cos\theta_{thrust}|$ was greater than 0.95. With these requirements the efficiency for the hadronic Z selection was larger than 95%. A total of 3.5 million hadronic events were selected.

Simulated events were produced by the JETSET 7.3 parton-shower generator [6] and then processed through a detailed simulation program, DELSIM, which modelled the detector response [4]. The simulated result from DELSIM was then processed by the same reconstruction program as used for the data, DELANA [4]. A total of 9.8 million Z$\to q\bar{q}$ events was simulated (11.8 million for the Ξ_b analysis).

In this simulation sample, there were only a few thousand $\Xi_c^0 \to \Xi^-\pi^+$ events, and about 1000 $\Xi_b \to \Xi\ell\bar{\nu}X$ events. Thus some dedicated Ξ_c^0 and Ξ_b samples were generated for the years 1992–1995 using the DELSIM and DELANA versions corresponding to each year. About 58 000 $\Xi_c^0 \to \Xi^-\pi^+$ events and 208 000 $\Xi_b \to \Xi\ell\bar{\nu}X$ events were simulated (see Table 1).

Year	Ξ_c^0 events	Ξ_b^- events	Ξ_b^0 events
1992	11 159	50 710	1 365
1993	12 142	52 735	1 331
1994	20 636	50 203	1 221
1995	13 874	49 378	1 227
Total	57 811	203 026	5 144

Table 1: *Number of simulated $\Xi_c^0 \to \Xi^-\pi^+$, Ξ_b^- and Ξ_b^0 events for each 1992–1995 year.*

4 Ξ^- reconstruction

The Ξ^- hyperon was reconstructed through the decay $\Xi^- \to \Lambda\pi^-$. A constrained multivertex fit to the three-dimensional decay topology was used to reconstruct the decay chain and suppress the combinatorial background.

In this analysis all V^0 candidates, i.e. all pairs of oppositely charged particles, were considered as Λ candidates. For each pair, the highest momentum particle was assumed to be a proton and the other a pion, and a vertex fit was performed by the standard DELPHI V^0 search algorithm [4]. The Λ candidates were selected by requiring: an invariant mass

$M(p\pi^-)$ between 1.107 GeV/c^2 and 1.125 GeV/c^2, a χ^2 probability of the V^0 vertex fit larger than 0.001 and an $R\phi$ decay length greater than 1.0 cm. To avoid gamma conversions, the relative transverse momentum, p_T, of the proton and pion had to be greater than 0.03 GeV/c, with p_T calculated with respect to the line joining the primary and secondary vertices. The angle in the xy-plane between the V^0 momentum and its line of flight had to be smaller than 0.08 radian. If the V^0 was reconstructed outside the VD, it was also required that no signal in the vertex detector could be consistently associated with the V^0 vertex tracks. In the following, the proton and pion from the Λ decay will be called p_1 and π_1, respectively, thus denoting $\Lambda = (p_1\pi_1^-)$.

The Λ's selected as described above were combined with pions (called π_2 in the following) with the same charge as the π_1 from the Λ. The π_2 candidate had not to be tagged as an electron or a muon.

A constrained multivertex fit [7,8] was performed if the invariant mass $M(\Lambda\pi_2^-)$ was smaller than 2.0 GeV/c^2 and if the distance between the two trajectories in the z direction was smaller than 2 cm at the point of crossing in the xy-plane. The fit used was a general least-squares fit with the following kinematical and geometrical constraints applied to each Ξ^- candidate:

- the invariant mass $M(p_1\pi_1^-)$ had to be equal to the nominal mass of the Λ;
- the $R\phi$ and z coordinates of p_1 and π_1 had to be the same at the radial distance of the Λ decay point;
- the $R\phi$ and z coordinates of Λ and π_2 had to be equal at the radial distance of the Ξ^- decay point;
- to ensure momentum conservation at the Ξ^- decay point, the polar and azimuthal angles of the Ξ^- candidate had to be equal to the angles from the curved trajectory between the decay and primary vertices. The curvature was calculated from the Ξ^- momentum.

For each of the three particles, i.e. the proton and pion from the Λ and the pion from the Ξ^-, the fit was performed with the following five track parameters: $1/r$ (r being the radius of curvature of the track), the z and $R\phi$ impact parameters, the polar angle θ, and the azimuthal angle ϕ. These 15 variables, plus the z coordinate of the primary vertex, were the measured variables in the fit. The x and y coordinates of the primary vertex were so precisely measured that they were taken as fixed. The unmeasured variables were the radial distances of the Ξ^- and Λ decay points, giving a total of 18 variables in the fit. The curved Ξ^- track was not measured, but calculated in the fit. All the tracks were corrected for ionization losses, according to the given mass hypothesis. The performance of the fit was tuned by adjusting the covariance matrices of the tracks. The adjustment consisted in a scaling of the errors of the track parameters. After the adjustment the pull distributions of the 16 fitted quantities were standard normal distributions within 10%.

The events for which the fit converged gave the $\Lambda\pi_2^-$ invariant-mass spectrum shown in Figure 1, The solid line is a fit, for illustrative purpose, using two Gaussian functions with the same mean for the signal, and a first order polynomial for the background, yielding 9445±584 Ξ^-.

5 Iterative discriminant analysis

Using sequential cuts to select the signal leads to what can be pictured as a multi-dimensional rectangular box in the parameter space. A more flexible separating surface can be obtained if the variables are combined in a polynomial instead. In this analysis a non-linear discriminant D of the form

$$D = \mathbf{x}^{\mathbf{T}}(\mathbf{a} + \mathbf{B}\mathbf{x}) = a_1 x_1 + ... + a_n x_n + B_{11} x_1^2 + ... + B_{1n} x_1 x_n + ... + B_{nn} x_n^2 \quad (1)$$

was defined [9], where x_i are the n variables used, and a_i and B_{ij} are the corresponding weights. This can be written as

$$D = \mathbf{c}^{\mathbf{T}}\mathbf{y} = c_1 y_1 + ... + c_m y_m, \quad (2)$$

where $\mathbf{c}$ contains all the weights a_i and B_{ij}, $\mathbf{y}$ is the vector $(\mathbf{x}, \mathbf{x} \cdot \mathbf{x}^{\mathbf{T}})$, and $m = (n^2 + 3n)/2$. To obtain a good signal-from-background separation, the variance of D should be as small as possible while the separation in D should be as large as possible. Therefore the ratio

$$\rho = \frac{(\mathbf{c}\Delta\boldsymbol{\mu})^2}{\mathbf{c}^{\mathbf{T}}\mathbf{V}\mathbf{c}} \quad (3)$$

was maximized. Here $\mathbf{V}$ is the sum of the signal and background variance matrices

$$\mathbf{V} = \mathbf{V}_{sig} + \mathbf{V}_{bkg} \quad (4)$$

and $\Delta\boldsymbol{\mu}$ is the difference between the signal and background arithmetic means:

$$\Delta\boldsymbol{\mu} = \boldsymbol{\mu}_{sig} - \boldsymbol{\mu}_{bkg} \quad (5)$$

of all the m variables in $\mathbf{y}$. The discriminant was calculated iteratively, and at each step of the iteration the variables x_i that gave the maximum background rejection were chosen. A chosen signal efficiency was used to determine the D-cuts after each step. The total number of variables used in the discriminant D, as well as the number of iterative steps, and the efficiency of each step, can be varied in the discriminant analysis. A large number of variations of the combinations of variables used in the discriminant, the number of steps, as well as the signal efficiencies, was investigated before deciding on which parameter combination to use.

6 Production of $\Xi^-\pi^+$ states

Each Ξ^- candidate in the mass range $1.30 < M(\Lambda\pi_2^-) < 1.34$ GeV/c^2, was combined with another pion, called π_3. It was required that π_3 should have a charge opposite to the π_1 from Λ decay, and should not be tagged as a lepton. For all $(\Xi^-\pi_3^+)$ combinations the invariant mass was calculated. If its value satisfied $2.2 < M(\Xi^-\pi_3^+) < 2.75$ GeV/c^2 (for Ξ_c^0), or $M(\Xi^-\pi_3^+) < 1.6$ GeV/c^2 (for $\Xi(1530)^0$), the iterative discriminant analysis described above was performed.

6.1 $\Xi_c^0 \rightarrow \Xi^-\pi^+$ selection

6.1.1 Separate simulation sets

Two separate sets of simulated events were needed. The training sample (called T(Ξ_c^0) in the following) was used to find the weight vector $\mathbf{c}$ that gave a maximum signal-from-background separation in D, while the analysis sample (called A(Ξ_c^0)) was used to determine the Ξ_c^0 efficiency (see Section 6.1.3). Both sets T(Ξ_c^0) and A(Ξ_c^0) consisted of signal as well as background events. The dedicated $\Xi_c^0 \rightarrow \Xi^-\pi^+$ events described in Section 3 were thus divided into two sets: about 2/3 of the events were used in set T(Ξ_c^0) and the rest in set A(Ξ_c^0). The simulated Z$\rightarrow q\bar{q}$ events were used for the background in both cases, using only events without any simulated Ξ_c^0's. The signal in set T(Ξ_c^0) consisted of about 36000 events, while the background corresponded to approximately $4.4 \cdot 10^6$ $q\bar{q}$ events. After the constrained fit, and the above-mentioned selections, about 1900 signal and 75000 background events remained in set T(Ξ_c^0) to be used for the discriminant training. Set A(Ξ_c^0) consisted of approximately 22000 $\Xi_c^0 \rightarrow \Xi^-\pi^+$ events, plus background events without any simulated Ξ_c^0 corresponding to $5.3 \cdot 10^6$ $q\bar{q}$ events. For each year, the number of background events in set A(Ξ_c^0) was weighted to correspond to the number of data events. Each of the years 1992–1995 was trained separately. The total numbers of events in the samples used for the (Ξ_c^0) analysis are shown in Table 2.

	MC T(Ξ_c^0)	MC A(Ξ_c^0)		Data
Signal	35 678	22 133		
After cuts	1 883	1 268		
Background	4 426 483	5 329 144	Total	3 498 492
After cuts	74 750	86 967	After cuts	57 291

Table 2: *The numbers of signal and background events in the simulation sets T(Ξ_c^0) and A(Ξ_c^0) (described in Section 6.1.1), and in the data, both before and after the multivertex fit and applied selections.*

6.1.2 Parameter optimization

As mentioned above, a large number of parameter combinations was investigated before a discriminant with two iterative steps, and seven variables, was chosen. The chosen variables were the momentum $p(\Xi_c^0)$, the fitted mass $M(\Xi^-)_{fit}$, the angle between Ξ^- and π_3^+, the b-tagging probability, the Λ decay length or the Ξ^- decay length, the momentum $p(\Xi^-)$ or the Λ mass, the impact parameter of the π_2^- or the momentum $p(\pi_2^-)$, with some variations among the different years.

6.1.3 Ξ_c^0 production

Using the discriminants D with the above mentioned variables on the simulation set A(Ξ_c^0), resulted in the $(\Lambda\pi^-\pi^+)$ invariant-mass distribution shown in Figure 2. An extended unbinned maximum-likelihood fit was performed. The likelihood function used had the form:

$$\log L = \log\left(\mu_s f_s + \mu_b f_b\right) - (\mu_s + \mu_b), \tag{6}$$

where f_s is a Gaussian function used to parametrize the signal and f_b, the probability density function for the background, is a first order polynomial. The numbers of signal and background events were given by μ_s and μ_b, respectively. The fit gave 498 ± 28 events with a σ width of 19$\pm$2 MeV/c^2 and mass $M(\Xi_c^0) = 2471 \pm 1$ MeV/c^2, which can be compared with the generated mass of 2473.0 MeV/c^2. The number of true Ξ_c^0 events in the peak was 494, and there was thus an excellent agreement.

The same discriminants were also used on the data, with the resulting mass distribution shown in Figure 3. In this case the fit gave 45$\pm$13 events with a σ width of 22$\pm$6 MeV/c^2. The mass from the fit was 2460$\pm$8 MeV/c^2, in agreement with the world average value $M(\Xi_c^0) = 2471.8 \pm 1.4$ MeV/c^2 [10].

The reconstruction efficiency is highly momentum dependent, and in order to avoid biases due to the Ξ_c^0 momentum distribution not having been correctly described by the simulation, the Ξ_c^0 rate was determined in two momentum bins, as shown in Table 3 and Figure 4. Integrating the observed distribution and using the JETSET generator [6] to estimate the fraction of events outside the observable momentum region (5.5%), a total rate of

$$f_{\Xi_c^0} \times \mathrm{BR}(\Xi_c^0 \to \Xi^-\pi^+) = (4.7 \pm 1.4(stat.)) \times 10^{-4} \qquad (7)$$

per hadronic Z decay was obtained.

Particle	x_p interval	Efficiency	Nb. of particles	$\frac{1}{N_{had}}\frac{dN}{dx_p}$
$\Xi_c^0 \to \Xi^-\pi^+$	0.10–0.40	(2.9±0.2)%	28.2±10.6	$(9.2 \pm 3.5) \times 10^{-4}$
	0.40–0.80	(1.9±0.2)%	11.0±6.5	$(4.1 \pm 2.4) \times 10^{-4}$
$\Xi(1530)^0 \to \Xi^-\pi^+$	0.015–0.10	(3.4±0.5)%	271.1±39.3	$(2.7 \pm 0.4) \times 10^{-2}$
	0.10–0.20	(7.6±0.9)%	293.1±37.5	$(1.1 \pm 0.1) \times 10^{-2}$
	0.20–0.50	(1.5±0.4)%	37.3±15.8	$(2.4 \pm 1.0) \times 10^{-3}$

Table 3: *The Ξ_c^0 and $\Xi(1530)^0$ differential production rates. The efficiency and number of particles from the fit in each of the $x_p = p/p_{beam}$ intervals are also given.*

6.2 $\Xi(1530)^0$ production

As for the Ξ_c^0 analysis, an iterative discriminant analysis was applied for the $\Xi(1530)^0$ selection, and two separate simulation sets were used. No special $\Xi(1530)^0$ simulation was needed, and the $q\overline{q}$ simulated events were used for both signal and background events.

The $\Xi(1530)^0$ discriminant analysis was applied to the simulation and resulted in the $(\Lambda\pi^-\pi^+)$ invariant-mass distribution shown in Figure 5. The same maximum likelihood function as for the Ξ_c^0 was used, except that the signal was described by a Breit-Wigner function, while the background was parametrized by [11]

$$F(x) = (x - x_0)^a \times \exp\left(b_0(x - x_0) + b_1(x - x_0)^2\right), \qquad (8)$$

where x is the invariant mass measured in GeV/c^2, x_0 is the kinematical limit of 1.4609 GeV/c^2, and a, b_0 and b_1 are free parameters. Since the signal peak is fairly close to the maximum of the background, the fit easily became unstable. Therefore the width Γ_0 in the Breit-Wigner was kept fixed at the world average value of 9.1±0.5 MeV/c^2 [10].

Performing the fit on the simulation resulted in 844 ± 71 signal events, and a mass of 1531.2 ± 0.5 MeV/c^2, in good agreement with the number of $\Xi(1530)^0$ events in the sample (831), and the generated mass of 1532.0 MeV/c^2.

Using the same discriminant on the 1992–1995 data sample gave the invariant mass spectrum shown in Figure 6. The unbinned maximum-likelihood fit gave 599 ± 57 signal events in the peak, with a mass of 1533.0 ± 0.5 MeV/c^2, which can be compared with the world average value $M(\Xi(1530)^0) = 1531.80 \pm 0.32$ MeV/c^2 [10]. The $\Xi(1530)^0$ production rate was evaluated in three momentum bins, as shown in Table 3 and Figure 4. Integrating the observed distribution and using the JETSET generator [6] to estimate the fraction of events outside the observable momentum region (7.7%), a total rate of

$$f_{\Xi(1530)^0} \times \mathrm{BR}(\Xi(1530)^0 \to \Xi^-\pi^+) = (4.5 \pm 0.5) \times 10^{-3} \qquad (9)$$

per hadronic Z decay was obtained.

6.3 Systematic uncertainties in production fractions

6.3.1 The Ξ_c^0 baryon

Several different sources of systematic uncertainties were investigated. The systematic uncertainty from the choice of the discriminant parameters was studied by varying the number of discriminant variables, the number of steps, and the signal efficiencies. No significant variation beyond the expected statistical fluctuation was found.

Due to the difference in the Ξ_c^0 momentum distribution in $c \to \Xi_c^0$ and $b \to c \to \Xi_c^0$ events, respectively, the reconstruction efficiencies in $c\bar{c}$ and $b\bar{b}$ events can also differ. An important contribution to the systematic error was therefore the uncertainty in the different c and b efficiencies, as well as the relative production of Ξ_c^0 in $c\bar{c}$ and $b\bar{b}$ events. The number of observed Ξ_c^0 particles, N_{seen}, is given by

$$N_{seen} = N \times (R_c \cdot f_c \cdot \epsilon_c + R_b \cdot f_b \cdot \epsilon_b) \times \mathrm{BR}, \tag{10}$$

where N is the total number of data events, R_c and R_b are the Z partial widths $\Gamma(c\bar{c})/\Gamma(hadrons)$ and $\Gamma(b\bar{b})/\Gamma(hadrons)$, ϵ_c and ϵ_b are the Ξ_c^0 reconstruction efficiencies for $c\bar{c}$ and $b\bar{b}$ events, $f_c = f(c\bar{c} \to \Xi_c^0)$ and $f_b = f(b\bar{b} \to \Xi_c^0)$ are the fractions of $c\bar{c}$ and $b\bar{b}$ quark pairs giving a Ξ_c^0, respectively (it has been assumed that Ξ_c^0 is only produced in $c\bar{c}$ and $b\bar{b}$ events). Finally, $\mathrm{BR} = \mathrm{BR}(\Xi_c^0 \to \Xi^-\pi^+)$ is the branching fraction for the studied channel.

The reconstruction efficiencies for $c\bar{c}$ and $b\bar{b}$ events were determined from the simulation and found to be $\epsilon_c = (1.4 \pm 0.2)\%$, and $\epsilon_b = (3.2 \pm 0.2)\%$. To estimate the relative weights of the f_c and f_b terms, both simulation and data events were used. The b-purity of the Ξ_c^0 sample was enhanced with a b-tag probability selection cut and $f_b \times \mathrm{BR}$ could then be found assuming that the contribution from $c\bar{c}$ events was negligible. The new b efficiency $\epsilon_b^{(b)}$ was found from the simulation. The number of fitted Ξ_c^0 in data after this selection, $N_{seen}^{(b)}$, was measured, and used to determine $f_b \times \mathrm{BR}$ from:

$$N_{seen}^{(b)} = N \times (R_b \cdot f_b \cdot \epsilon_b^{(b)}) \times \mathrm{BR}. \tag{11}$$

It was found that $f_b \times \mathrm{BR} = (1.3 \pm 0.6) \times 10^{-3}$, essentially independent of the chosen b-tag cut.

Using this value in equation 10, f_c/f_b was found to be compatible with 1. For the study of the systematic uncertainty $f_b \times \mathrm{BR}$ was varied by one statistical standard deviation, while f_c/f_b was varied between 0.5 and 2.0 in equation 10. The systematic uncertainty was thus estimated to be $\pm 1.0 \times 10^{-4}$.

Other sources of systematics came from the contribution of the finite simulation statistics to the uncertainty on the total Ξ_c^0 efficiency, and the error rescaling done in the multivertex fit, giving a systematic uncertainty of $\pm 0.3 \times 10^{-4}$ from each source.

As already mentioned, the JETSET model was used to estimate the fraction of events in the unobserved momentum regions, which was found to be 5.5%. The comparison with JETSET (Figure 4) shows a good agreement, thus the systematic uncertainty was estimated by varying the value from the simulation by ±50%, resulting in a systematic uncertainty contribution of $\pm 0.2 \times 10^{-4}$.

All the above systematics are summarized in Table 4. These uncertainties were then added in quadrature, which gave the final result:

$$f_{\Xi_c^0} \times \mathrm{BR}(\Xi_c^0 \to \Xi^-\pi^+) = (4.7 \pm 1.4(stat.) \pm 1.1(syst.)) \times 10^{-4}. \tag{12}$$

Source	$f\times$BR(Ξ_c^0)	$f\times$BR($\Xi(1530)^0$)
Finite MC statistics	0.3×10^{-4}	0.4×10^{-3}
MC extrapolation	0.2×10^{-4}	0.2×10^{-3}
multivertex fit	0.3×10^{-4}	0.4×10^{-3}
b, c efficiencies	1.0×10^{-4}	—
Total	1.1×10^{-4}	0.6×10^{-3}

Table 4: *The different contributions to the total systematic uncertainty for* Ξ_c^0 *and* $\Xi(1530)^0$*, as described in Section 6.3.*

6.3.2 The $\Xi(1530)^0$ baryon

The systematic uncertainties for $\Xi(1530)^0$ were studied in the same way as for the Ξ_c^0 events, except that since the $\Xi(1530)^0$ mainly comes from the fragmentation, these results were not affected by the flavour of the leading quark. All the different uncertainty contributions, summarized in Table 4, were then added in quadrature, and the final $\Xi(1530)^0$ result was

$$f_{\Xi(1530)^0} \times \mathrm{BR}(\Xi(1530)^0 \to \Xi^-\pi^+) = (4.5 \pm 0.5(stat.) \pm 0.6(syst.)) \times 10^{-3}, \qquad (13)$$

in agreement with the world average value of $(5.3 \pm 1.3) \times 10^{-3}$ [10] and the results of DELPHI [12] and OPAL [11]. The $\Xi(1530)^0$ result was used as a cross-check of the analysis method.

7 Update of the Ξ_b production rate and lifetime

The strange b-baryon Ξ_b was searched for in the semileptonic decay channel, $\Xi_b \to \Xi^-\ell^-\bar{\nu}X$. In the semileptonic decays of heavy hadrons the flavour of the spectator system of the initial state is transmitted to the final state. This property can be used to study Ξ_b baryons from the observation of $\Xi^\mp$ production accompanied by a lepton of the same sign. The occurrence of $\Xi^\mp - \ell^\mp$ pairs of same sign ("right sign") is then compared to that of opposite sign pairs, $\Xi^\mp - \ell^\pm$ ("wrong sign").

7.1 Ξ^- and lepton reconstruction

The Ξ^- was reconstructed using a constrained multivertex fit as in the Ξ_c^0 analysis. If the fit was successful, the Ξ^- candidate was combined with a lepton candidate (electron or muon) within 1.0 radian of the Ξ^- momentum vector. Since the expected production rate of the Ξ_b is very small, loose selections were applied to the Ξ^- and Λ candidates. The discriminant analysis method described above was used for the final Ξ_b selection. Five variables were used in the discriminant; the transverse momentum of the lepton with respect to the jet axis, the invariant mass of the Ξ^- and lepton, the combined momentum of the Ξ^- and lepton, the number of charged particles in a 0.31 radian cone around the lepton direction and the Ξ^- variable, $\xi = -\ln x_p$, where $x_p = p_\Xi/p_{beam}$.

When applied to the Monte Carlo analysis sample, consisting of 1/3 of the simulated events, the discriminant method gave the resulting $\Lambda\pi$ invariant-mass distributions of Figure 7. Applying the extended unbinned maximum-likelihood fit described in Section 6.1.3 to the two distributions, with a Gaussian function for the Ξ^--peak and a constant value for the background, gave 34.2±5.9 right-sign events, and 11.3±3.5 wrong-sign events, when normalised to the size of the data sample. The number of true Ξ_b events in the right-sign Ξ^- mass peak was 25.6. Here the mass peak region was defined as the region with reconstructed Ξ^- mass within ±10 MeV/c^2 of the nominal Ξ^- mass.

The same analysis was applied to the full DELPHI 1992–1995 data sample and the resulting $\Lambda\pi$ invariant-mass distributions are shown in Figure 8. The unbinned maximum-likelihood fit to the two distributions, gave a mean value of 1321.0±0.8 MeV/c^2 for the right-sign distribution, compatible with the nominal Ξ^- mass (1321.31 ± 0.13 MeV/c^2 [10]). The mean value from the fit to the right-sign distribution was used as a fixed parameter in the fit to the wrong-sign distribution. The maximum-likelihood fit resulted in 28.3±5.8 right-sign events, and 7.6±3.3 wrong-sign events.

7.2 Ξ_b production rate

The number of background events in the right-sign Ξ^- mass peak was estimated from that in the wrong-sign mass peak, which resulted in 20.7 ± 6.7 Ξ_b events found in the data. According to the simulation, the number of background events is equal in the right- and wrong-sign Ξ^- mass peaks. In the Monte Carlo analysis sample the same procedure gave 23.0 ± 6.8 events to be compared with the number of true $\Xi_b \to \Xi^-\ell^-X$ events in the right-sign mass peak which was 25.6.

The total Ξ_b efficiency, calculated from the Ξ_b signal simulation sample, was $(2.3 \pm 0.1)\%$. Using the measured fraction of Z$\rightarrow b\bar{b}$ relative to all Z hadronic decays, R_b = $(21.650 \pm 0.072)\%$ [10], leads to a Ξ_b production rate of:

$$\mathrm{BR}(b \to \Xi_b) \times \mathrm{BR}(\Xi_b \to \Xi^-\ell^-X) = (3.0 \pm 1.0(stat.)) \times 10^{-4} \quad (14)$$

per lepton species, averaged for electrons and muons.

The dominating source of systematic uncertainty was the contribution of Λ_b to the background. The uncertainty in the background contribution of Λ_b was estimated by varying the amount of these events in the background by ±20% of the value in the simulation [10]. This gave a shift of $\pm 0.20 \times 10^{-4}$ of the production rate. Other sources of systematic uncertainty were the finite simulation statistics, the error rescaling done in the multivertex fit, the Monte Carlo extrapolation of the events into the unobserved momentum regions (9.3%) and a possible Ξ_b polarisation. All the above sources of systematic uncertainty are summarized in Table 5. The final result for the Ξ_b production rate was:

$$\mathrm{BR}(b \to \Xi_b) \times \mathrm{BR}(\Xi_b \to \Xi^-\ell^-X) = (3.0 \pm 1.0(stat.) \pm 0.3(syst.)) \times 10^{-4} \quad (15)$$

per lepton species, averaged for electrons and muons. This measurement of the production rate is in agreement with the previous measurements done by DELPHI [1] using a smaller data sample, and by ALEPH [2], see Table 6. In the previous DELPHI analysis [1], the background was estimated from the simulation while in this analysis the background was estimated using the wrong-sign data sample.

7.3 Ξ_b lifetime

The final sample of $\Xi^-\ell^-$ events is also used to measure the Ξ_b lifetime. The secondary vertex from the Ξ_b semileptonic decay is obtained by use of the BSAURUS package [13]. The secondary vertex in the hemisphere is calculated in BSAURUS using tracks that are likely to have originated from the decay chain of a weakly decaying b-hadron state. The

Source	Production rate variation
Finite MC stat.	0.10×10^{-4}
Multivertex fit	0.15×10^{-4}
MC extrapolation	0.15×10^{-4}
Ξ_b polarisation	0.14×10^{-4}
MC model of background	0.20×10^{-4}
Total	0.3×10^{-4}

Table 5: *The different contributions to the total systematic uncertainty of the Ξ_b production rate, as described in Section 7.2.*

Reference	Production rate
ALEPH [2]	$(5.4 \pm 1.1(stat.) \pm 0.8(syst.)) \times 10^{-4}$
DELPHI [1]	$(5.9 \pm 2.1(stat.) \pm 1.0(syst.)) \times 10^{-4}$
this analysis	$(3.0 \pm 1.0(stat.) \pm 0.3(syst.)) \times 10^{-4}$

Table 6: *Comparison between different results for the Ξ_b production rate.*

vertex fitting is done in three dimensions, using the constraint of the direction of the b-hadron candidate momentum vector, p_b. The decay-length estimate in the $R\phi$ plane, is defined as the distance between the primary- and secondary-vertex positions if the secondary-vertex fit was successful. The three-dimensional decay length is obtained as $L = L_{R\phi}/\sin\theta$, where θ is the polar angle of the b-hadron candidate. The sign of the decay length is determined by the direction of the $\Xi\ell$ momentum vector: the distance is positive if the secondary vertex is found beyond the primary vertex in this direction. The resulting proper-time estimate for the Ξ_b candidates is given by $t = L\, m_{\Xi_b}/p_b$, where the Ξ_b rest mass is taken to be 5.8 GeV/c^2.

The lifetime was determined by an unbinned maximum-likelihood fit to the proper time distribution.

The background was taken as the wrong-sign combinations plus the right-sign combinations outside the mass peak but with a reconstructed Ξ^- mass between 1.280 GeV/c^2 and 1.363 GeV/c^2. Both signal and background lifetimes were fitted simultaneously. The purity in the right-sign mass peak was fixed in the fit and was taken from the simulation to be 0.67.

In the 1992–1995 DELPHI data sample, 29 events in the right-sign mass peak remained after the secondary vertex fit. The statistical overlap of one event with the previous DELPHI lifetime measurement was removed. The result of the lifetime fit on the DELPHI data is presented in Figure 9, and gave $\tau_{\Xi_b} = 1.45^{+0.55}_{-0.43}(stat.)$ ps. The exact composition of the background, and the lifetimes of its individual components, had no effect on the signal lifetime since the background lifetime was fitted on the data. Varying the fraction of Ξ_b in the right-sign peak between 0.60 and 0.74 resulted in a variation of the fitted Ξ_b lifetime of ±0.10 ps. The proper time resolution was varied by $\pm50\%$, which resulted in a shift of ±0.07 ps. The effect of a possible Ξ_b polarisation was studied and found to be small. Finally the Ξ_b lifetime was measured to be

$$\tau_{\Xi_b} = 1.45^{+0.55}_{-0.43}(stat.) \pm 0.13(syst.) \text{ ps.} \tag{16}$$

The measurement is in agreement with the previous measurements done by DELPHI [1] and by ALEPH [2], see Table 7.

Reference	Lifetime (ps)
ALEPH [2]	$1.35^{+0.37}_{-0.28}(stat.)^{+0.15}_{-0.17}(syst.)$
DELPHI [1]	$1.5^{+0.7}_{-0.4}(stat.) \pm 0.3(syst.)$
this analysis	$1.45^{+0.55}_{-0.43}(stat.) \pm 0.13(syst.)$

Table 7: *Comparison between different results for the Ξ_b lifetime.*

The earlier DELPHI lifetime measurement [1] used the data from 1991–1993 and a different method to reconstruct the Ξ^--hyperon and the proper time, and the background lifetime was estimated using simulation. A combination of the two DELPHI lifetime measurements gives

$$\tau_{\Xi_b} = 1.48^{+0.40}_{-0.31}(stat.) \pm 0.12(syst.) \text{ ps}, \tag{17}$$

using the method outlined in [14]. The systematics are uncorrelated.

8 Summary and conclusions

The production rate per hadronic Z decay for the charmed baryon Ξ_c^0 has been measured for the first time:

$$f_{\Xi_c^0} \times \text{BR}(\Xi_c^0 \to \Xi^-\pi^+) = (4.7 \pm 1.4(stat.) \pm 1.1(syst.)) \times 10^{-4}.$$

As a cross-check, the $\Xi(1530)^0$ resonance was also reconstructed, and the corresponding production rate was found to be:

$$f_{\Xi(1530)^0} \times \text{BR}(\Xi(1530)^0 \to \Xi^-\pi^+) = (4.5 \pm 0.5(stat.) \pm 0.6(syst.)) \times 10^{-3},$$

in agreement with previous results [10].

The beauty strange baryon Ξ_b was searched for in the semileptonic decay channel $\Xi_b \to \Xi^-\ell^-X$. The product of the branching ratios in b and Ξ_b decays was measured to be:

$$\text{BR}(b \to \Xi_b) \times \text{BR}(\Xi_b \to \Xi^-\ell^-X) = (3.0 \pm 1.0(stat.) \pm 0.3(syst.)) \times 10^{-4}$$

per lepton species, averaged for electrons and muons.

A measurement of the Ξ_b lifetime gave:

$$\tau_{\Xi_b} = 1.45^{+0.55}_{-0.43}(stat.) \pm 0.13(syst.) \text{ ps},$$

in agreement with earlier results [1,2]. A combination of the two DELPHI lifetime measurements gives

$$\tau_{\Xi_b} = 1.48^{+0.40}_{-0.31}(stat.) \pm 0.12(syst.) \text{ ps}.$$

Acknowledgements

We are greatly indebted to our technical collaborators, to the members of the CERN-SL Division for the excellent performance of the LEP collider, and to the funding agencies

for their support in building and operating the DELPHI detector.
We acknowledge in particular the support of
Austrian Federal Ministry of Education, Science and Culture, GZ 616.364/2-III/2a/98,
FNRS–FWO, Flanders Institute to encourage scientific and technological research in the industry (IWT), Belgium,
FINEP, CNPq, CAPES, FUJB and FAPERJ, Brazil,
Czech Ministry of Industry and Trade, GA CR 202/99/1362,
Commission of the European Communities (DG XII),
Direction des Sciences de la Matière, CEA, France,
Bundesministerium für Bildung, Wissenschaft, Forschung und Technologie, Germany,
General Secretariat for Research and Technology, Greece,
National Science Foundation (NWO) and Foundation for Research on Matter (FOM), The Netherlands,
Norwegian Research Council,
State Committee for Scientific Research, Poland, SPUB-M/CERN/PO3/DZ296/2000, SPUB-M/CERN/PO3/DZ297/2000, 2P03B 104 19 and 2P03B 69 23(2002-2004)
FCT - Fundação para a Ciência e Tecnologia, Portugal,
Vedecka grantova agentura MS SR, Slovakia, Nr. 95/5195/134,
Ministry of Science and Technology of the Republic of Slovenia,
CICYT, Spain, AEN99-0950 and AEN99-0761,
The Swedish Research Council,
Particle Physics and Astronomy Research Council, UK,
Department of Energy, USA, DE-FG02-01ER41155.
EEC RTN contract HPRN-CT-00292-2002.

References

[1] DELPHI Collab., P. Abreu *et al.*, Zeit. Phys. **C68** (1995) 541.
[2] ALEPH Collab., D. Buskulic *et al.*, Phys. Lett. **B384** (1996) 449.
[3] DELPHI Collab., P. Aarnio *et al.*, Nucl. Instr. and Meth. **A303** (1991) 233.
[4] DELPHI Collab., P. Abreu *et al.*, Nucl. Instr. and Meth. **A378** (1996) 57.
[5] DELPHI Collab., J. Abdallah *et al.*, Eur. Phys. J. **C32** (2004) 185.
[6] T. Sjöstrand, Comp. Phys. Comm. **82** (1994) 74.
[7] DELPHI Collaboration, W. Adam et al., Z. Phys. **C70** (1996) 371.
[8] V. Blobel, "Least squares methods", in Formulae and Methods in Experimental Data Evaluation, Vol 3, R. K. Bock et al. (Ed.).
[9] T.G.M. Malmgren, Comp. Phys. Comm. **106** (1997) 230.
[10] Particle Data Group, Phys. Rev. **D66** (2002) 010001.
[11] OPAL Collab., G. Alexander *et al.*, Zeit. Phys. **C73** (1997) 569.
[12] DELPHI Collab., P. Abreu *et al.*, Zeit. Phys. **C67** (1995) 543.
[13] Z. Albrecht et al., "BSAURUS - A Package For Inclusive B-Reconstruction in DELPHI", hep-ex/0102001.
[14] L. Di Ciaccio *et al.*, "Averaging Lifetimes for B Hadron Species", Oxford University preprint OUNP 96-05 (1996), Rome University preprint ROM2F/96/09 (1996), Max Planck Institute Munich MPI-Phe/96-05 (1996).

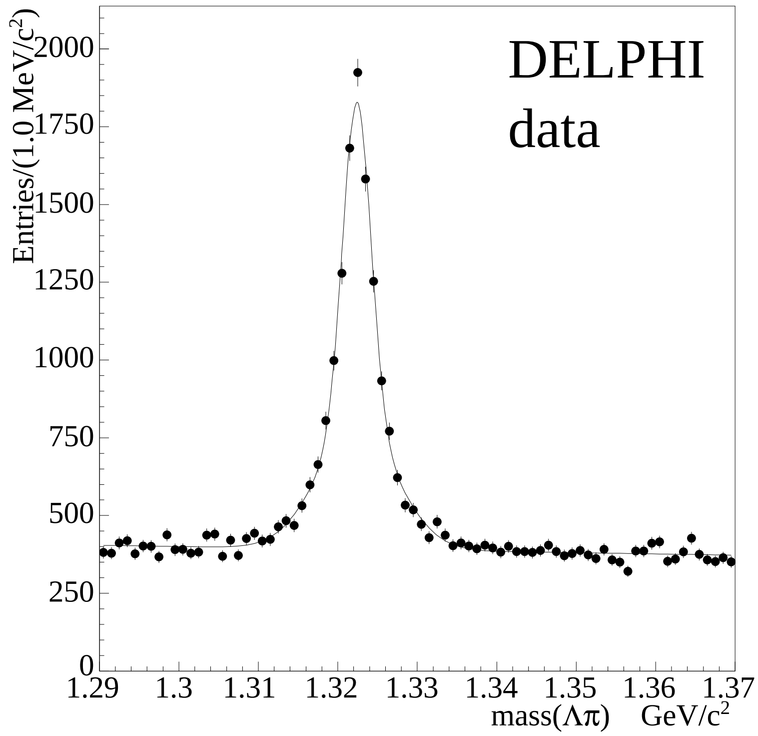

Figure 1: *The* $\Lambda\pi^-$ *invariant-mass spectrum, using a constrained fit on the 1992–1995 data sample. The curve is the result of a fit using a first-order polynomial to parametrize the background and two Gaussian functions of same mean for the signal.*

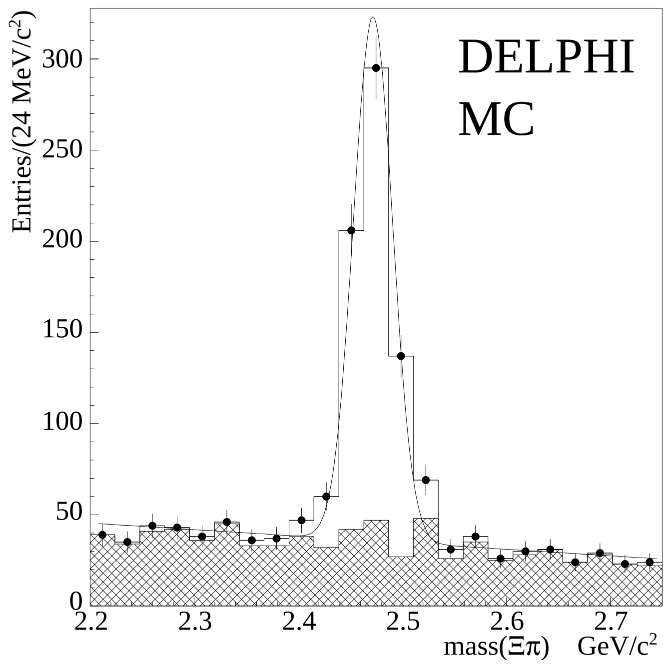

Figure 2: *The $\Lambda\pi^-\pi^+$ invariant-mass spectrum in the 1992–1995 simulation. The background (cross-hatched histogram) corresponds to $5.3 \cdot 10^6$ $Z\rightarrow q\bar{q}$ simulated events. The signal (white histogram) consists of about 22000 $\Xi_c^0 \rightarrow \Xi^-\pi^+$ simulated events. The fitted curve, as described in Section 6.1.3, uses a first-order polynomial to parametrize the background and a Gaussian function for the signal.*

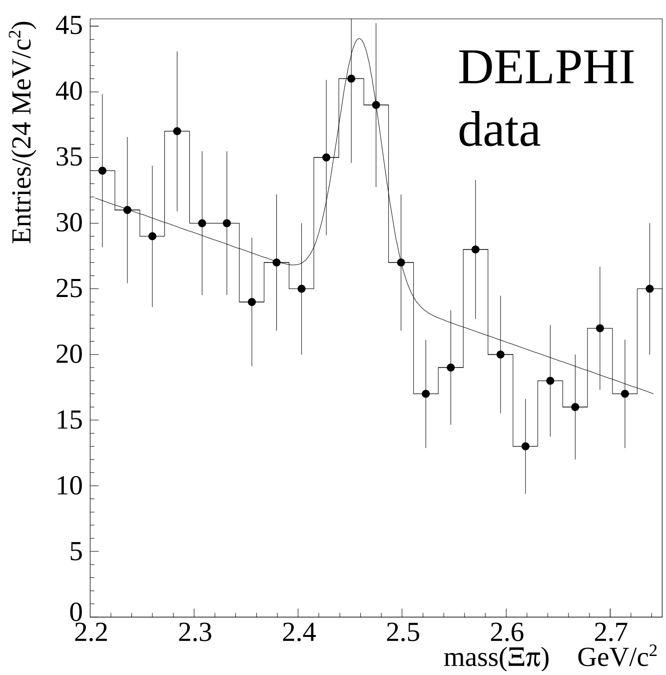

Figure 3: *Same as Figure 2 for the 1992–1995 data sample, corresponding to* $3.5 \cdot 10^6$ *hadronic Z decays.*

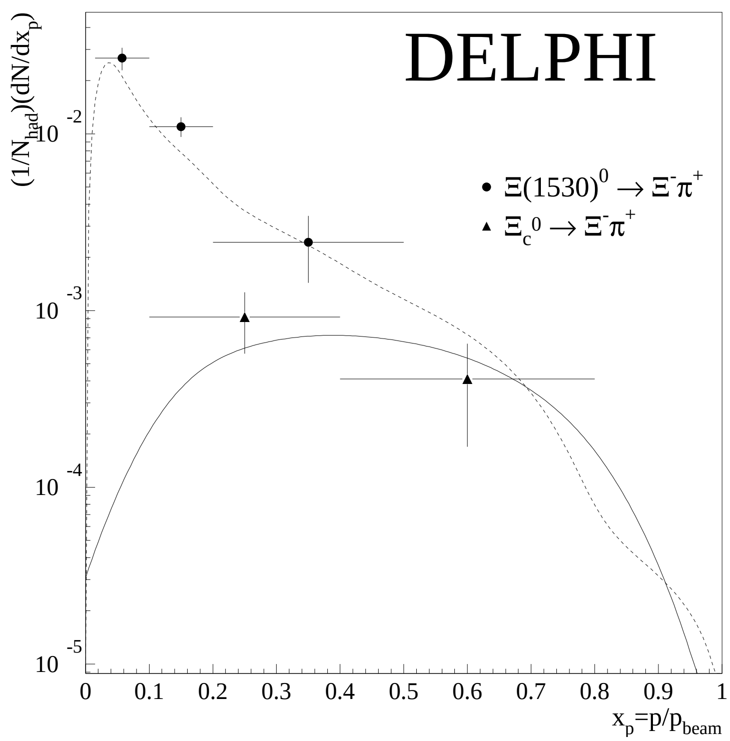

Figure 4: *The measured differential production rates for* Ξ_c^0 *(plotted as triangles), and* $\Xi(1530)^0$ *(circles). For comparison the JETSET 7.4 [6] prediction is shown, with a full line for* Ξ_c^0*, and a dashed line for* $\Xi(1530)^0$*.*

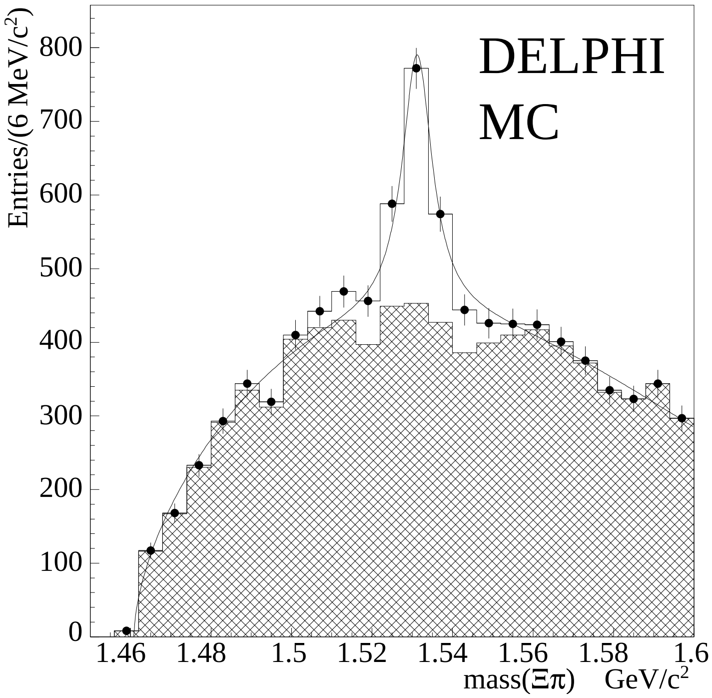

Figure 5: *The* $\Lambda\pi^{-}\pi^{+}$ *invariant-mass spectrum, using* $5.3 \cdot 10^{6}$ *simulated hadronic Z decays. The background events are cross-hatched. The fitted curve, as described in Section 6.2, uses a parametrized background and a Breit-Wigner function for the signal.*

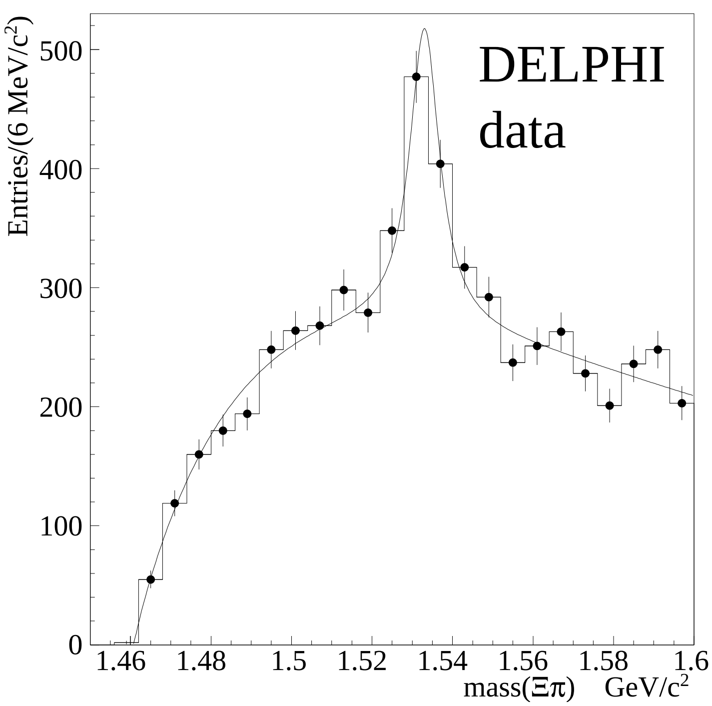

Figure 6: *Same as Figure 5 for the 1992–1995 data sample, corresponding to* $3.5 \cdot 10^{6}$ *hadronic Z decays.*

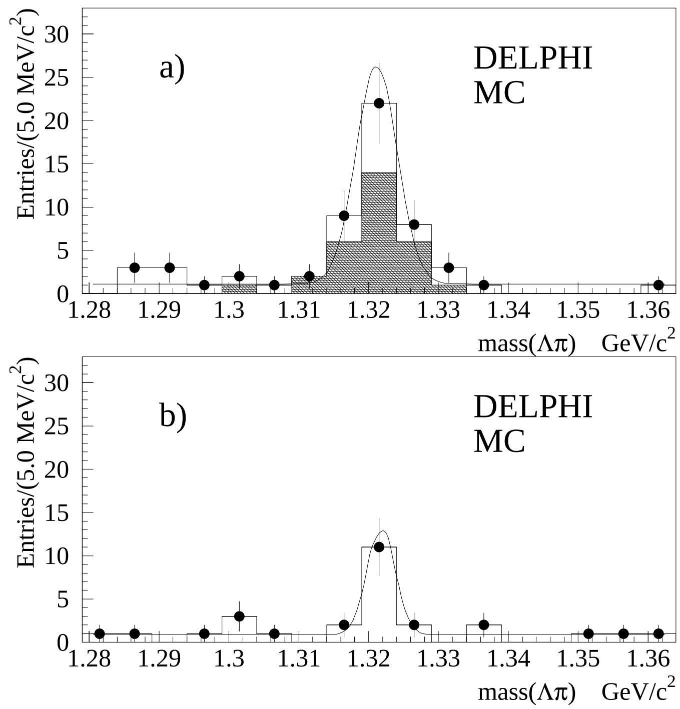

Figure 7: *The $\Lambda\pi^-$ invariant-mass spectrum, using 3.8 million simulated hadronic Z decays: a) $\Xi^\mp - \ell^\mp$ right-sign pairs, b) $\Xi^\mp - \ell^\pm$ wrong-sign pairs. The true Ξ_b simulated events are grey hatched. The two fitted curves, as described in Section 7.1, each uses a constant value to parametrize the background and a Gaussian function for the Ξ^- peak.*

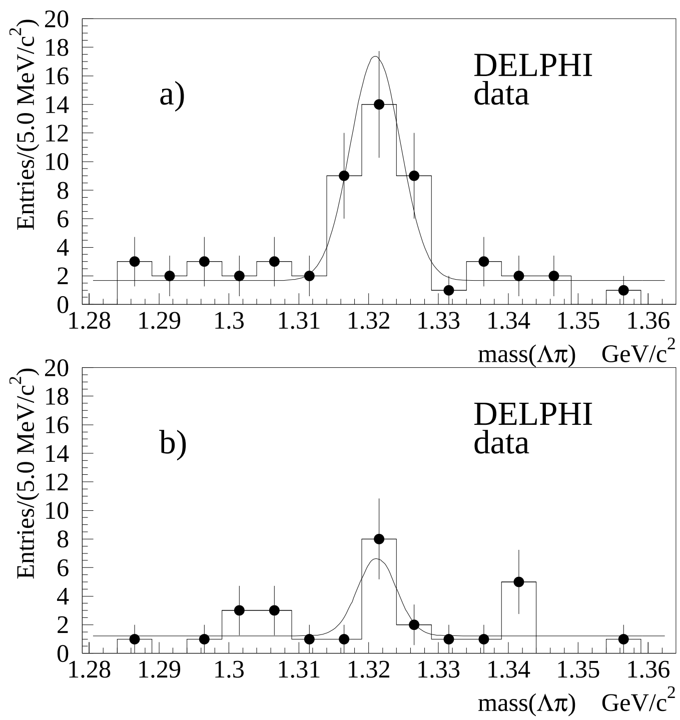

Figure 8: *Same as Figure 7 for the 1992–1995 data sample, corresponding to* $3.5 \cdot 10^6$ *hadronic Z decays.*

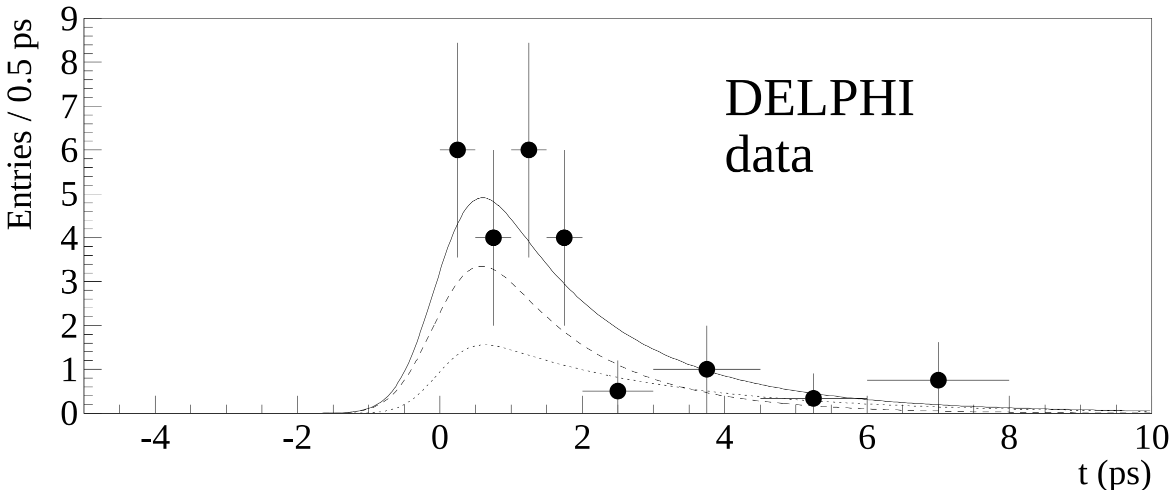

Figure 9: *The result of the lifetime fit to the selected Ξ_b events in the data sample. The dotted curve is for the background, and the dashed line corresponds to the signal. The full line is the total.*